HHS Public Access

Author manuscript

Biochem Biophys Res Commun. Author manuscript; available in PMC 2023 March 17.

Published in final edited form as:

Biochem Biophys Res Commun. 2022 January 08; 587: 146–152. doi:10.1016/j.bbrc.2021.11.100.

Lysyl hydroxylase 2 deficiency promotes filopodia formation and fibroblast migration

Ryunosuke Nozaki[a], **Atsushi Kasamatsu**[b,*], **Joel Moss**[c], **Katsuhiro Uzawa**[a,b,**]

[a]Department of Oral Science, Graduate School of Medicine, Chiba University, Chiba, Japan

[b]Department of Dentistry and Oral-Maxillofacial Surgery, Chiba University Hospital, Chiba, Japan

[c]Pulmonary Branch, National Heart, Lung, and Blood Institute, National Institutes of Health, Bethesda, MD, USA

Abstract

Lysyl hydroxylase 2 (LH2) regulates intermolecular cross-linking of collagen molecules. Accumulation of LH2-modified collagen, which is highly stable and resistant to collagenase cleavage, is one cause of fibrosis. We previously demonstrated that conventional LH2 knockout mice showed embryonic lethality. Here we established LH2 conditional knockout mice using a tamoxifen-inducible Cre system. Morphological analysis of LH2-deficient fibroblasts by microscopy showed a dramatic increase in the number of filopodia, the finger-like cell surface projections that enable cell movement. The tips and leading edges of these filopodia exhibited up-regulated expression of Myosin-X (Myo10), a regulator of filopodial integrity. Wound healing assays demonstrated that migration of LH2-deficient cells was significantly faster than that of control cells. Gene expression profiling data also supported this phenotype. Together these findings indicate that LH2 deficiency may prevent fibrosis through decreased accumulation of LH2-cross-linked collagen, and that fibroblasts with faster migration contribute to enhanced wound healing activity. In conclusion, our cellular models provide evidence that LH2 deficiency plays a critical role in cell migration mediated through filopodia formation. Understanding the precise role of this phenotype in LH2-deficient cells may be helpful to define the pathogenesis of fibrosis. As such, detailed analyses of fibrosis and wound healing using LH2-deficient mouse models are needed.

[*]Corresponding author. Department of Oral Science, Graduate School of Medicine, Chiba University, 1-8-1 Inohana, Chuo-ku, Chiba-shi, Chiba, 260-8670, Japan. kasamatsua@faculty.chiba-u.jp (A. Kasamatsu). [**]Corresponding author. Department of Oral Science, Graduate School of Medicine, Chiba University, Chiba, Japan. uzawak@faculty.chiba-u.jp (K. Uzawa).

Author contributions

K.U. and A.K. designed and directed the study. R.N. performed the majority of the experiments. R.N. and A.K. contributed to the biochemical analyses, interpreted the data and the overall results. R.N., A.K., J.M., K.U. reviewed the experimental data, drafted the manuscript and revised the figures. All authors discussed the results and contributed to the final manuscript.

Declaration of competing interest

The authors declare that they have no known competing financial interests or personal relationships that could have appeared to influence the work reported in this paper.

Appendix A. Supplementary data

Supplementary data to this article can be found online at https://doi.org/10.1016/j.bbrc.2021.11.100.

Keywords

Lysyl hydroxylase 2; Conditional knockout; Filopodia; Cell migration; Fibroblast Mouse; Wound healing

1. Introduction

Lysyl hydroxylation of collagens, catalyzed by members of the lysyl hydroxylase family (LH1–3), is a critical post-translational modification for development and stability of connective tissues [1–3]. LH1 mediates lysyl hydroxylation in the helical domain of collagen molecules. LH2 catalyzes formation of telopeptidyl hydroxylysine and LH3 functions primarily as a glucosyltransferase. The importance of lysyl hydroxylation is highlighted by the role of LH1–3 deficiencies in inheritable disorders, such as Ehlers-Danlos syndrome type VI, Bruck syndrome, and Epidermolysis bullosa-like syndromes, respectively [4].

LH2 expression is universally up-regulated in fibrosis [5–7]. LH2-mediated hydroxylation of telopeptidyl lysine residues in collagen initiates formation of hydroxylysine aldehyde-derived collagen cross-links (HLCCs), which are highly stable and resistant to cleavage by collagenases [5,6,8–11]. Increased LH2 expression under pathological conditions can promote accumulation of collagen with HLCCs in the extracellular matrix, ultimately leading to fibrosis and organ failure [5,6,12]. Inhibition of LH2 enzymatic activity leads to reversible fibrosis, but does not interfere with normal repair processes [12]. On the other hand, increased LH2 expression contributes to metastasis in breast cancer, lung cancer, and sarcoma, highlighting the therapeutic potential of LH2 inhibitors to combat both cancers and fibrosis [13].

Our previous study demonstrated that mice with conventional knockout (KO) of LH2 showed embryonic lethality at E10.5 with abnormal heart wall morphology [14]. In the present study, we established for the first time a mouse with conditional KO (cKO) of LH2 using a tamoxifen-inducible Cre system to prevent embryonic lethality. We describe a novel cellular phenotype associated with cell migration in LH2-deficient cells from these mice.

2. Materials and methods

2.1. Construction of a targeting vector for LH2

A floxed allele of LH2 was generated in collaboration with Cyagen Biosciences (Guangzhou, China) using traditional gene targeting methods. Using a positive BAC clone from the C57BL/6 J library, a targeting vector carrying the long homology arm including exon 3, the short homology arm, the conditional knockout (cKO) recombination sites, and selection markers was constructed. The neomycin cassette was flanked by two FRT sites and exon 2 was flanked by two loxP sites (Fig. 1A). Restriction analyses with the restriction endonucleases *Hind*III and *Bam*HI were performed to confirm the structure of the targeted LH2 allele. Cre-mediated DNA recombination was confirmed by sequencing (Fig. 1B).

2.2. Generation of LH2 $^{F/F}$ CAG-Cre mice

To excise the neomycin cassette, LH2$^{T/+}$ mice were mated with Flp recombinase transgenic mice to generate LH2$^{F/+}$ mice (Fig. 1A). The recombinase protein (Cre) recognizes loxP sequences and catalyzes recombination of LH2 exon 2 between the two loxP sites. CAG-Cre mice treated with tamoxifen ubiquitously express Cre recombinase, which can delete the floxed gene in all tissues. Interbreeding between heterozygous LH2$^{F/+}$ mice and CAG-Cre mice generated LH2 $^{F/+}$ CAG-Cre mice. The LH2$^{F/+}$ mice were then intercrossed with LH2 $^{F/+}$ CAG-Cre mice to generate LH2 $^{F/F}$ CAG-Cre mice.

2.3. Tail tissue fibroblasts (TTF)

After euthanasia, mouse tails were skinned and minced into 1-cm pieces, which were then placed on 30-mm tissue culture dishes coated with collagen I and containing Dulbecco's Modified Eagle's Medium (DMEM without sodium pyruvate; Nacalai Tesque, Kyoto, Japan), 10% fetal bovine serum (FBS; Sigma-Aldrich, St. Louis, MO, USA), and 50 units/ml penicillin. The plates were maintained at 37 °C with 5% CO_2.

2.4. Polymerase chain reaction (PCR)

Genomic DNA was extracted from mouse tails and TTFs using a MonoFas Genomic DNA Extraction kit (GL Sciences Inc.), according to the manufacturer's protocol. Cre-mediated DNA recombination was determined by PCR. Primers were designed using Primer3Plus [15], which specified the optimal primer set. The primers used are shown in Supplemental Table. PCR was carried out in a 50 μl reaction volume containing 0.25 μl Ex Taq polymerase (TaKaRa), 4 μl dNTP mix (TaKaRa), 1 μl of each primer, 5 μl Ex Taq buffer (TaKaRa), 5 μl cDNA, and 33.75 μl nuclease-free water. The reaction was performed at 94 °C for 3 min, followed by 33 cycles of 94 °C for 30 s, 60 °C for 35 s, 72 °C for 35 s, and a final extension cycle at 72 °C for 5 min. PCR product size was determined by electrophoresis on 2% agarose gels.

2.5. Reverse transcription PCR (RT-PCR)

Total RNA was isolated with TRIzol reagent (Invitrogen, Carlsbad, CA, USA). Analysis of the LH2 expression level in TTFs was evaluated by RT-PCR. Primers were designed using Primer3Plus, which specifies the optimal primer set. The primers are shown in Supplemental Table. The size of the amplified product for wild type and cKO LH2 is 275 bp and 183 bp, respectively.

2.6. Western blot analysis

Cell lysates containing 20 μg protein were separated on NuPAGE Tris-Acetate Pre-Cast Gels (Invitrogen) under denaturing conditions and the proteins were subsequently transferred to PVDF membranes (Bio-Rad) by electroblotting. The membranes were blocked with Blocking One (Nacalai Tesque) for 1 h at room temperature, and then incubated overnight at 4 °C with the following primary antibodies: 1:1000; anti-rabbit LH2, # 21214-1-AP (Proteintech, Rosemont, IL, USA) and 1:200; anti-rabbit GAPDH #sc-25778 (Santa Cruz Biotechnology, Santa Cruz, CA, USA). After washing the membranes with 0.1% Tween-20 in Tris-buffered saline (TBS-T) three times, the membranes were incubated with horseradish

peroxidase (HRP)-conjugated IgG as a secondary antibody (Promega, Madison, WI, USA) at room temperature. Finally, the membranes were visualized using a ChemiDoc XRS Plus System (Bio-Rad, Hercules, CA, USA) with Image Lab software (Bio-Rad).

2.7. Proliferation assay

TTFs from $LH2^{F/F}$ and $LH2^{F/F}$ CAG-Cre mice were placed in 6-well plates at 1×10^4 cells/well. The indicated doses of tamoxifen were added to TTF cultures for 72 h. The cells were counted every 24 h using a Luna Automated Cell Counter (Logos Biosystems, Annandale, VA, USA). All experiments were performed in triplicate.

2.8. Immunocytochemistry

TTFs were fixed in 0.1% paraformaldehyde, 2 mM $MgCl_2$, and 1 mM EDTA in culture medium at room temperature for 20 min, washed twice with culture medium, and permeabilized with culture medium containing 0.5% Triton X-100 at room temperature for 10 min. TTFs were washed twice with culture medium and blocked with culture medium containing 5% BSA (Gibco-BRL, Waltham, MA, USA) for 30 min. The cells were incubated with Myo10 antibody (Bio-Rad) for 1 h, washed three times with culture medium, and then incubated with anti-rabbit fluorescein isothiocyanate (FITC)-conjugated secondary antibody for 1 h. For F-actin staining, cells were incubated with 5 U/ml rhodamine phalloidin (Sigma-Aldrich) at room temperature for 20 min. To visualize cell nuclei, the cells were counterstained with DAPI. Images were captured from each surface using a *Keyence BZ-X800 microscope with Keyence* software.

2.9. Wound-healing assay

To investigate cell migration, 70% confluent TTF monolayers were scraped in a single straight line using a sterile 200 μl pipette tip. After washing with PBS, the cells were refreshed with medium and incubated at 37 °C for 6, 12, and 24 h, respectively. Initial (0 h) and residual (6, 12, and 24 h) gap lengths were calculated based on photomicrographs.

2.10. Transwell-chamber assay

Quantification of cell migration was carried out using transwell chambers with 8 μm pore size. TTFs (1×10^5) were cultured on the upper layer with serum-free medium and incubated for 6,12, and 24 h. Simultaneously, the lower layer was filled with DMEM containing 10% FBS. Cells remaining on the upper side of the membrane were removed with a cotton swab, and cells migrating to the bottom side of the membrane were fixed with 4% paraformaldehyde and stained with 0.1% crystal violet. The number of stained cells in five randomly selected areas was counted using an inverted microscope, and the average value was used to determine the cell migration activity.

2.11. Time-lapse video microscopy

For cell migration assays, TTFs were placed on a stage incubator of a *Keyence BZ-X800 (Keyence Corporation, Osaka, Japan)* microscope at 37 °C and 5% CO_2. Images were captured every 15 min for 24 h with phase-contrast optics at a magnification of 20×. Time-lapse videos were assembled using *Keyence* software and imported into the BZ-X800

Analyzer for analysis and cropping. To calculate migratory distances, TTFs were tracked using the time-lapse macro in the VW-9000 Motion Analyzer.

2.12. Microarray analysis

The mRNA expression profiles of LH2 cKO TTFs were screened using a SurePrint G3 Mouse GE microarray (Agilent Technologies, Santa Clara, CA, USA). Total RNA was extracted from cells with TRIzol Reagent (Invitrogen) and the SV Total RNA Isolation System (Promega), according to the manufacturer's instructions. RNA samples were quantified by an ND-1000 spectrophotometer (NanoDrop Technologies, Wilmington, DE, USA) and the quality was confirmed with an Experion System (Bio-Rad). The cRNA was amplified, labeled, and hybridized to a 60 K Agilent 60-mer oligo-microarray, according to the manufacturer's instructions. All hybridized microarray slides were scanned using an Agilent scanner. Relative hybridization intensities and background hybridization values were calculated using Agilent Feature Extraction Software (9.5.1.1). Raw signal intensities and Flags for each probe were calculated from hybridization intensities and spot information, according to procedures recommended by Agilent. The raw signal intensities for all samples were normalized by a quantile algorithm with the 'preprocessCore' library package of Bioconductor software [16,17]. To identify genes having up- or down-regulated expression, we calculated signals and ratios (non-log scaled fold-change) from normalized signal intensities of each probe for comparison between control and experimental samples. The microarray data can be accessed through the NCBI GEO accession viewer (GSE186100). Expression intensity values for genes having significant differential expression were obtained based on a fold-change cutoff greater than 2.0 or less than 0.5. Gene Set Enrichment Analysis (GSEA; http://www.broadinstitute.org/gsea/index.jsp) was carried out using the Gene Ontology (GO) migration and cell-cell adhesion gene sets. Gene sets were considered to be significantly enriched with $P < 0.05$ and FDR <0.25.

3. Results

3.1. Establishment of LH2$^{F/F}$ CAG-Cre

We first established LH2$^{F/F}$ CAG-Cre mice to obtain LH2 cKO cells. Genomic DNA from ES cells after homologous recombination was digested with *Hind*III or *Bam*HI. Southern blot analysis showed that wild type and mutant LH2 alleles (LH2^{T}) were obtained after homologous recombination in ES cells (Fig. 1A). The neomycin cassette probe detected 17 kb (*Hind*III digestion) and 8 kb (*Bam*HI digestion) DNA fragments on Southern blotting analysis of 6 positive clones (Fig. 1A). After obtaining LH2$^{F/F}$ CAG-Cre mice, we confirmed Cre-mediated DNA recombination by tamoxifen treatment. Deletion of exon 2 of LH2 in LH2$^{F/F}$ CAG-Cre TTFs was confirmed by sequencing (Fig. 1B), PCR for genomic DNA (Fig. 1C), RT-PCR (Fig. 1D), and Western blot analyses (Fig. 1E).

3.2. Effect of tamoxifen on cell proliferation

To assess the effects of tamoxifen on cell growth, a cell proliferation assay with LH2$^{F/F}$ CAG-Cre TTFs was performed using the indicated tamoxifen dose. Treatment of LH2$^{F/F}$ CAG-Cre TTFs with 5 μM tamoxifen had no substantial effects on cell proliferation, whereas incubation with high doses (10–25 μM) of tamoxifen did influence cell growth

(Fig. 2A). We further compared cell growth between $LH2^{F/F}$ and $LH2^{F/F}$ CAG-Cre TTFs using 5 μM tamoxifen in a time-dependent manner. Since 5 μM tamoxifen did not affect proliferation of either $LH2^{F/F}$ or $LH2^{F/F}$ CAG-Cre TTFs (Fig. 2D), we used 5 μM tamoxifen as the test concentration.

3.3. Cre-mediated DNA recombination after treatment with tamoxifen in a time-dependent manner

To investigate tamoxifen-induced, Cre-mediated DNA recombination, we assessed LH2 mRNA and protein levels in $LH2^{F/F}$ CAG-Cre TTFs after treatment with 5 μM tamoxifen for the indicated time period. LH2 mRNA and protein expression were reduced at 12 h after tamoxifen treatment (Fig. 2B and C).

3.4. Assessment of LH2 cKO TTF cell morphology

To assess the effects of LH2 deficiency on cell morphology, live cell imaging was performed using a Keyence BZ-X800 (Keyence) microscope. Surprisingly, the number of filopodia seen for LH2 cKO TTFs was significantly greater than that seen for other cells (Fig. 2E, arrows). Filopodia formation involves actin structure reorganization, which is regulated by several actin-binding proteins, particularly Myo10 [18]. To study the mechanism underlying Myo10-induced actin rearrangement and filopodia formation, we performed immunocytochemistry with an anti-Myo10 antibody. Myo10 overexpression localized to the tip of filopodia in LH2 cKO TTFs was observed (Fig. 2F).

3.5. Effect of LH2 cKO on cell migration (wound healing assay)

Since LH2 cKO TTFs demonstrated filopodia generation and fibroblasts play a central role in healing of skin wounds, we performed *in vitro* scratch wound-healing assays in $LH2^{F/F}$ CAG-Cre TTFs in the presence or absence of tamoxifen treatment. Relative to control cells, significant wound closure was seen at both 12 h and 24 h for LH2 cKO TTFs (Fig. 3A; $P < 0.05$).

3.6. Effect of LH2 cKO on cell migration (transwell-migration assay)

To further investigate the effect of tamoxifen on cell migration in LH2 cKO TTFs, we performed a transwell-migration assay, which showed that LH2 cKO significantly promoted cell migration at 24 h after tamoxifen treatment (Fig. 3B; $P < 0.05$).

3.7. Time-lapse image of TTF migration

Live cell migration was analyzed using a Keyence BZ-X800 (Keyence) microscope. Migration distances seen for LH2 cKO cells were significantly greater than that for controls (Fig. 3C; $P < 0.05$). LH2 cKO TTFs exhibited filopodia generation in the leading edges of moving cells (Fig. 3D). To investigate dynamic features of TTF behavior, images were taken every 15 min (Supplementary video).

Supplementary video related to this article can be found at https://doi.org/10.1016/j.bbrc.2021.11.100

3.8. Gene expression analysis of LH2 cKO TTFs

To identify genes that are closely related to cell migration, we performed global screening of differentially expressed genes between control and LH2 cKO TTFs (Fig. 4A). Microarray analysis showed that 1600 genes were differentially expressed in tamoxifen-treated LH2 cKO TTFs compared to untreated $LH2^{F/F}$ CAG-Cre TTFs. Of these, 753 showed up-regulated expression of more than 2-fold, and 847 showed more than 2-fold downregulation in expression (Fig. 4A). In particular, *Myo1*0 mRNA expression was up-regulated in LH2 cKO TTFs compared with controls. Using GO term analysis of biological processes, the differentially expressed genes were significantly related to migration, and included those involved in cell projection organization, cell adhesion, cell morphogenesis, cell-cell adhesion, cell shape, and filopodium assembly (Fig. 4B). In addition, GSEA indicated significant enrichment in genes associated with migration and cell-cell adhesion (Fig. 4C). The results of these global gene expression analyses strongly supported our data showing that LH2 cKO affects filopodia generation that in turn enhances higher migration activity.

4. Discussion

Our previous study demonstrated that conventional LH2-KO mice showed embryonic lethality due to heart failure [14]. In the present study, we obtained LH2-deficient mice using a cKO system. Since LH2 has an important role in embryonic development, we first determined the cellular phenotype of LH2-deficient fibroblasts. LH2-deficient cells showed enhanced cell migration, resulting from increased filopodia formation following activation of Myo10 (Fig. 2E and F).

Filopodia are found in a variety of cell types [19]. Our data show that Myo10 localizes to filopodial tips and is found at the leading edge of LH2-deficient cells in a wound-healing assay. LH2-deficient cells extend filopodia toward the wound and use the filopodia to pull into the wound. Several actin-regulatory proteins, including Myo10, regulate filopodia formation and dynamics [19–21]. Forced dimerization of Myo10 induces filopodia formation, indicating that the motor activity of Myo10 is sufficient to initiate filopodia. Therefore, myosin activity can modulate cell migration velocity and direction [22]. Myo10 is essential for filopodia formation and has been found to directly bind to and transport integrins to the tips of filopodia for attachment [19,23,24]. Our data showed that Myo10 expression was up-regulated in LH2-deficient cells, where it promotes migration into wounds. The strong peripheral localization of Myo10 in the LH2-deficient cells suggests that LH2 deficiency may stimulate Myo10 activity directly, resulting in a large number of filopodia in LH2-deficient cells that can promote cell migration during wound healing.

LH2 expression is universally up-regulated in fibrosis [6,25]. LH2 forms strong collagen bonds that are not easily disrupted. Collagen formed in the presence of LH2 has been shown to initiate formation of HLCCs, which are stable and resistant to collagenase activity [5,6,8,9,11]. The enhanced LH2 expression seen in fibrosis could promote additional synthesis of these strong collagen cross-linked bonds to cause accumulation of HLCCs in the extracellular matrix. In internal organs, such as liver, lung, and kidney [12], enhanced fibrosis may block vital biological functions, leading to death.

High levels of LH2 expression can also contribute to the pathogenesis of several types of cancer and, in particular, metastasis of lung and breast cancers [13]. Overexpression of LH2 in cancer plays a critical role as a stabilizer of integrin β1 function, enabling integrin β1 to initiate tumor invasion and metastasis [20,24]. In contrast to our data for LH2-deficient cells, Ueki et al. reported that LH2 knockdown in cancer cells led to decreased cell migration by destabilizing integrin β1 [26]. Therefore, further experiments to examine differences in LH2 function between cancer cells and normal fibroblasts are needed to elucidate the role of LH2 in cancers.

In conclusion, the present study revealed that LH2-deficient cells showed dramatic increases in the number of filopodia having up-regulated Myo10 expression that leads to enhanced cell migration. As fetal fibroblasts, which migrate faster than adult fibroblasts, have an increased capacity to promote wound healing [27–29], understanding the precise phenotype of LH2-deficient cells will help define the relationship between LH2 enzymatic activity and pathogenesis of LH2-related disorders. Detailed analyses using LH2-deficient mouse models will be valuable for examining the mechanism of LH2 in disease pathogenesis.

Supplementary Material

Refer to Web version on PubMed Central for supplementary material.

Acknowledgements

We thank JAM Post (https://www.jamp.com/svcs/) for proof-reading this paper. JM was supported by the Intramural Research Program, National Institutes of Health, National Heart, Lung, and Blood Institute.

Data availability

Data will be made available on request.

References

[1]. Hautala T, et al. , Cloning of human lysyl hydroxylase: complete cDNA-derived amino acid sequence and assignment of the gene (PLOD) to chromosome 1p36.3–p36.2, Genomics 13 (1992) 62–69. [PubMed: 1577494]

[2]. Yeowell HN, Walker LC, Tissue specificity of a new splice form of the human lysyl hydroxylase 2 gene, Matrix Biol. 18 (1999) 179–187. [PubMed: 10372558]

[3]. Valtavaara M, Szpirer C, Szpirer J, Myllylä R, Primary structure, tissue distribution, and chromosomal localization of a novel isoform of lysyl hydroxylase (lysyl hydroxylase 3), J. Biol. Chem. 273 (1998) 12881–12886.

[4]. Ha-Vinh R, et al. , Phenotypic and molecular characterization of Bruck syndrome (Osteogenesis imperfecta with contractures of the large joints) caused by a recessive mutation in PLOD2, Am. J. Med. Genet. 131 (2004) 115–120. A. [PubMed: 15523624]

[5]. Van Der Slot AJ, et al. , Increased formation of pyridinoline cross-links due to higher telopeptide lysyl hydroxylase levels is a general fibrotic phenomenon, Matrix Biol. 23 (2004) 251–257. [PubMed: 15296939]

[6]. Van der Slot AJ, et al. , Identification of PLOD2 as telopeptide lysyl hydroxylase, an important enzyme in fibrosis, J. Biol. Chem. 278 (2003) 40967–40972.

[7]. Zuurmond AM, Van Der Slot-Verhoeven AJ, Van Dura EA, De Groot J, Bank RA, Minoxidil exerts different inhibitory effects on gene expression of lysyl hydroxylase 1, 2, and 3:

implications for collagen cross-linking and treatment of fibrosis, Matrix Biol. 24 (2005) 261–270. [PubMed: 15908192]

[8]. Jain N, et al. , Conditional knockout of N-WASP in mouse fibroblast caused keratinocyte hyper proliferation and enhanced wound closure, Sci. Rep. 6 (2016) 1–13. [PubMed: 28442746]

[9]. Mercer DK, Nicol PF, Kimbembe C, Robins SP, Identification, expression, and tissue distribution of the three rat lysyl hydroxylase isoforms, Biochem. Biophys. Res. Commun. 307 (2003) 803–809. [PubMed: 12878181]

[10]. Pornprasertsuk S, Duarte WR, Mochida Y, Yamauchi M, Lysyl hydroxylase-2b directs collagen cross-linking pathways in MC3T3-E1 cells, J. Bone Miner. Res. 19 (2004) 1349–1355. [PubMed: 15231023]

[11]. Uzawa K, et al., Differential Expression of Human Lysyl Hydroxylase in Vitro, 1999, 14, 1272–1280.

[12]. Piersma B, Bank RA, Collagen cross-linking mediated by lysyl hydroxylase 2: an enzymatic battlefield to combat fibrosis, Essays Biochem. 63 (2019) 377–387. [PubMed: 31324706]

[13]. Devkota AK, et al. , Development of a high-throughput lysyl hydroxylase (LH) assay and identification of small-molecule inhibitors against LH2, SLAS Discov. 24 (2019) 484–491. [PubMed: 30589612]

[14]. Kasamatsu A, et al. , Deficiency of lysyl hydroxylase 2 in mice causes systemic endoplasmic reticulum stress leading to early embryonic lethality, Biochem. Biophys. Res. Commun. 512 (2019) 486–491. [PubMed: 30905411]

[15]. Untergasser A, et al. , Primer3Plus, an enhanced web interface to Primer3, Nucleic Acids Res. 35 (2007) 71–74.

[16]. Gentleman RC, et al. , Bioconductor: open software development for computational biology and bioinformatics, Genome Biol. 5 (2004).

[17]. Bolstad BM, Irizarry RA, Astrand M, Speed TP, Gene expression omnibus A comparison of normalization methods for high density oligonucleotide array data based on bias and variance, Bioinformatics 19 (2003) 185–193. [PubMed: 12538238]

[18]. Ropars V, et al. , The myosin X motor is optimized for movement on actin bundles, Nat. Commun. 7 (2016).

[19]. He K, Sakai T, Tsukasaki Y, Watanabe TM, Ikebe M, Myosin X is recruited to nascent focal adhesions at the leading edge and induces multi-cycle filopodial elongation, Sci. Rep. 7 (2017) 1–12. [PubMed: 28127051]

[20]. Bohil AB, Robertson BW, Cheney RE, Myosin-X is a molecular motor that functions in filopodia formation, Proc. Natl. Acad. Sci. U. S. A. 103 (2006) 12411–12416.

[21]. Tokuo H, Ikebe M, Myosin X transports Mena/VASP to the tip of filopodia, Biochem. Biophys. Res. Commun. 319 (2004) 214–220. [PubMed: 15158464]

[22]. Knecht DA, Xue F, Janzen DM, Contribution of filopodia to cell migration: a mechanical link between protrusion and contraction, Int. J. Cell Biol. 2010 (2010).

[23]. Zhang H, et al. , Myosin-X provides a motor-based link between integrins and the cytoskeleton, Nat. Cell Biol. 6 (2004) 523–531. [PubMed: 15156152]

[24]. Vicente-Manzanares M, Choi CK, Erratum Horwitz AR, Integrins in cell migration – the actin connection (Journal of Cell Science vol. 122 (199–206, J. Cell Sci. 122 (2009) 1473.

[25]. Remst DFG, et al. , TGF-ß induces Lysyl hydroxylase 2b in human synovial osteoarthritic fibroblasts through ALK5 signaling, Cell Tissue Res. 355 (2014) 163–171. [PubMed: 24192939]

[26]. Ueki Y, et al. , PLOD2 is essential to functional activation of integrin β1 for invasion/metastasis in head and neck squamous cell carcinomas, iScience 23 (2020) 100850.

[27]. Rodrigues M, Kosaric N, Bonham CA, Gurtner GC, Wound healing: a cellular perspective, Physiol. Rev. 99 (2019) 665–706. [PubMed: 30475656]

[28]. Hu MS, et al. , Tissue engineering and regenerative repair in wound healing, Ann. Biomed. Eng. 42 (2014) 1494–1507. [PubMed: 24788648]

[29]. Rowlatt U, Intrauterine wound healing in a 20 week human fetus, Virchows Arch. A Pathol. Anat. Histol. 381 (1979) 353–361. [PubMed: 155931]

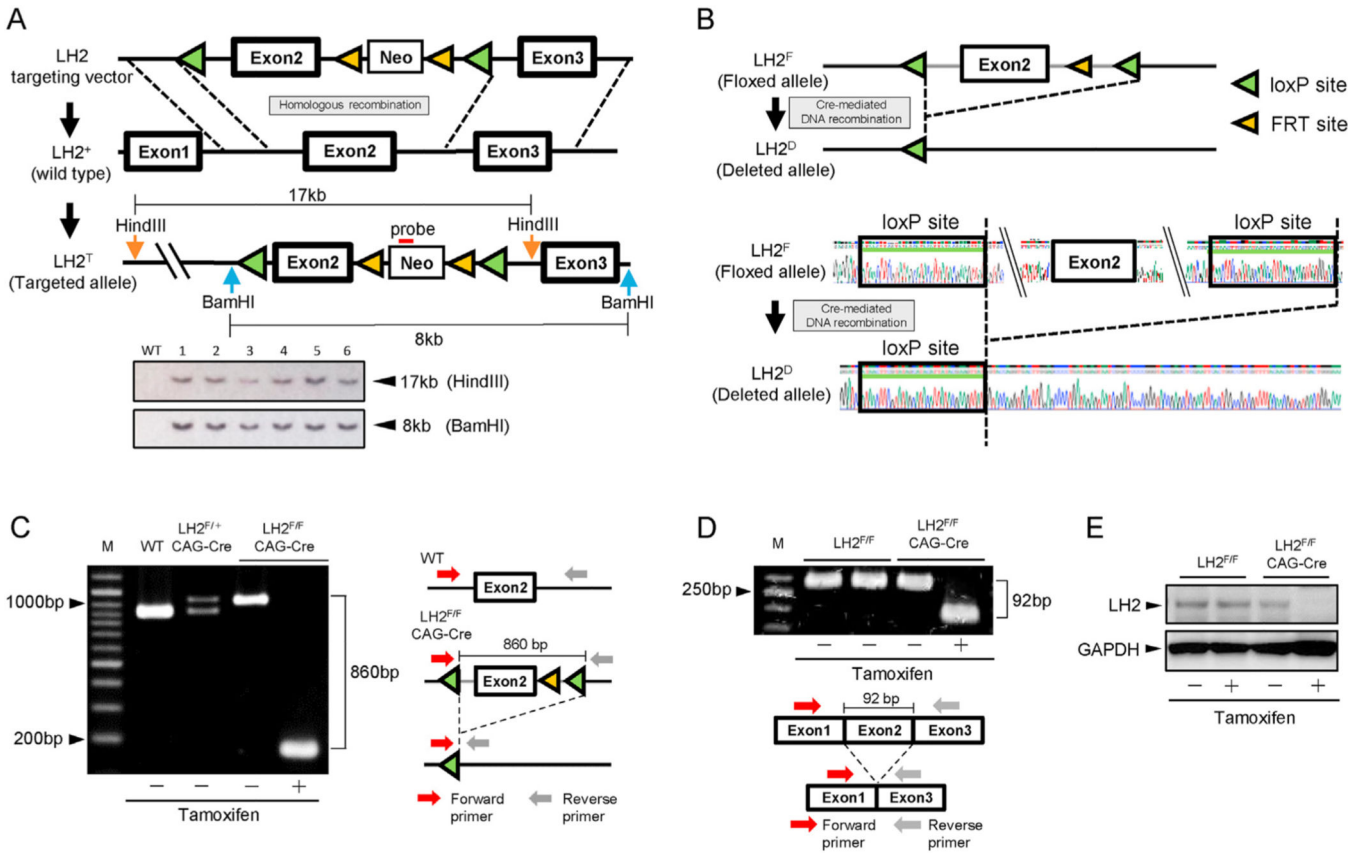

Fig. 1.

Establishment of $LH2^{F/F}$ CAG-Cre. **A,** Homologous recombination using a vector targeting LH2. The targeted LH2 allele ($LH2^{T}$) is identified in ES cells by Southern blot analysis. **B,** Confirmation of LH2 allele deletion ($LH2^{D}$) after CRE-mediated DNA recombination. Sequence results show DNA deletion of LH2-exon2. **C,** Confirmation of LH2 cKO TTFs by PCR of genomic DNA. **D,** Confirmation of LH2 cKO TTFs by RT-PCR. **E,** Confirmation of LH2 cKO TTFs by Western blot analysis.

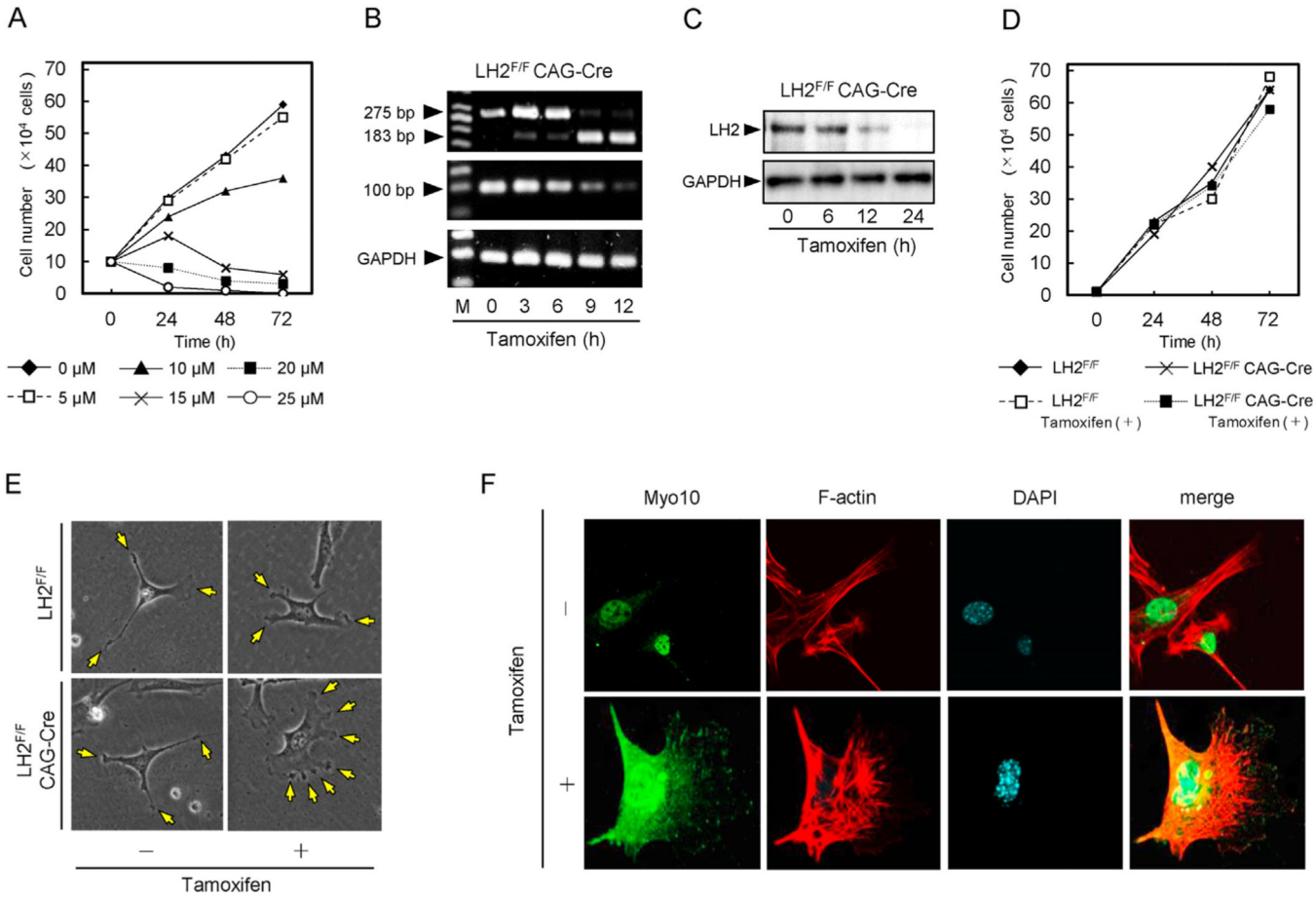

Fig. 2.

Effect of tamoxifen on LH2$^{F/F}$ CAG-Cre TTF proliferation and cell morphology. **A,** Effect of tamoxifen on proliferation of LH2$^{F/F}$ CAG-Cre TTFs in the presence of the indicated tamoxifen dose. Data are mean ± SEM of values obtained from 3 experiments conducted in triplicate. **B,** mRNA levels by RT-PCR in LH2$^{F/F}$ CAG-Cre TTFs after 5 μM tamoxifen treatment for the indicated time period. RT-PCR was performed to detect LH2 expression in LH2 cKO TTFs using LH2-exon2 and GAPDH specific primers (Supplemental Table). **C,** Western blot analysis of LH2 protein levels by in LH2$^{F/F}$ CAG-Cre TTFs after 5 μM tamoxifen treatment for the indicated time period. **D,** Comparison of cell growth between LH2$^{F/F}$ and LH2$^{F/F}$ CAG-Cre TTFs with/without 5 μM tamoxifen. Data are mean ± SEM of values obtained from 3 experiments conducted in triplicate. **E,** Representative images of migrating TTFs from LH2$^{F/F}$ and LH2$^{F/F}$ CAG-Cre with/without 5 μM tamoxifen. Yellow arrowheads indicate filopodia. **F,** Immunocytochemistry of LH2$^{F/F}$ CAG-Cre with/without 5 μM tamoxifen. LH2$^{F/F}$ CAG-Cre TTFs were subjected to immunolabeling with anti-Myo10 (green), fluorescent phalloidin (red), and DAPI (blue). (For interpretation of the references to colour in this figure legend, the reader is referred to the Web version of this article.)

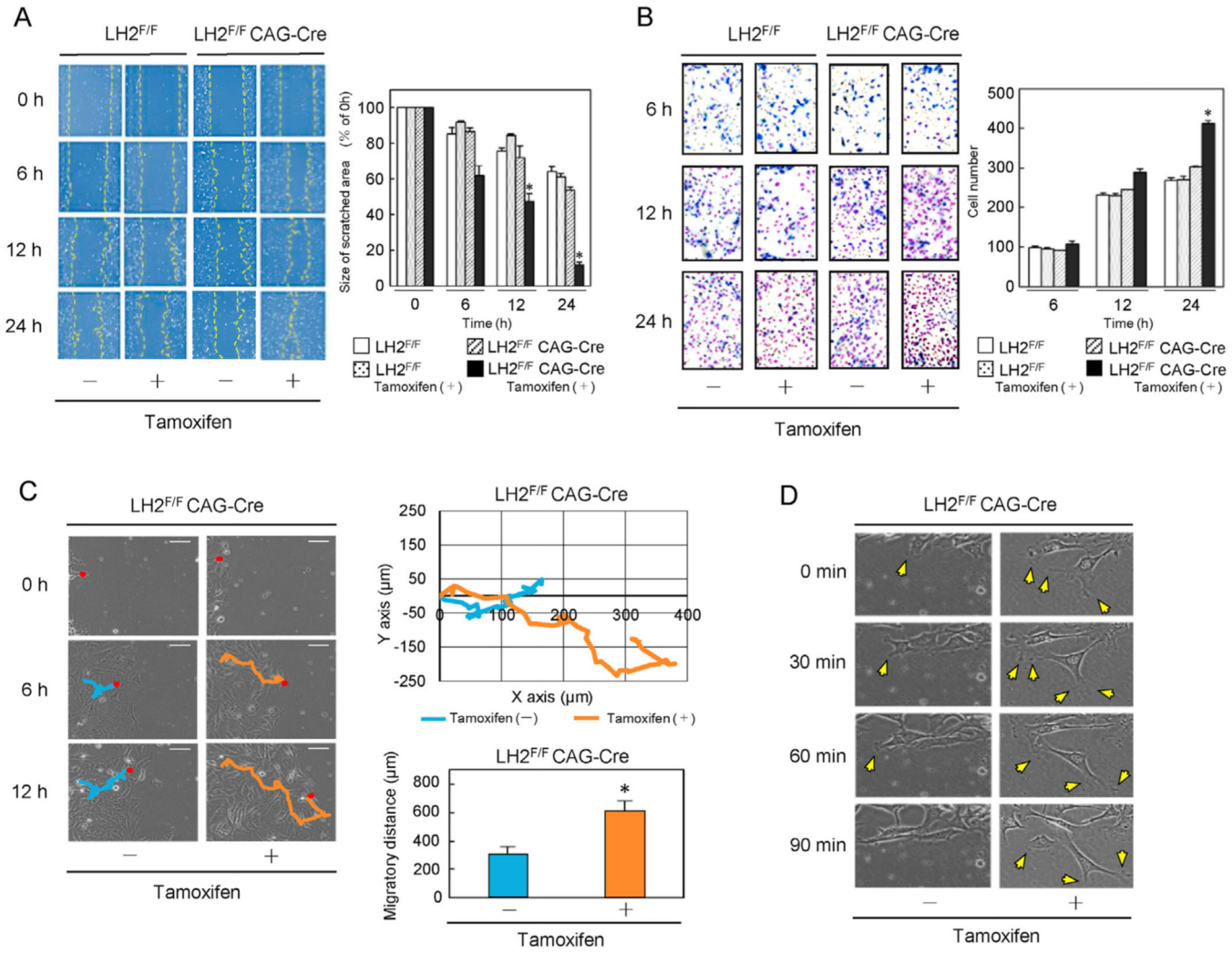

Fig. 3.

Effect of tamoxifen on LH2$^{F/F}$ CAG-Cre TTF migration. **A,** Representative images of recovery of scratched areas mediated by cell migration at 6, 12, and 24 h after tamoxifen treatment. Data for wound-healing assays expressed as the mean ± SEM of results for three independent experiments (*P < 0.05). **B,** Representative images for transwell migration assays taken 6, 12, and 24 h after tamoxifen treatment. Data for transwell-migration assays expressed as the mean ± SEM of results from three independent experiments (*P < 0.05). **C,** Representative image from time-lapse video at 12 h. Migration trajectories of the marked cells (blue and orange) are shown. Plotted data for migrating TTFs from time-lapse image recording for 12 h (blue, LH2$^{F/F}$ CAG-Cre TTF without tamoxifen; orange, LH2$^{F/F}$ CAG-Cre TTF with tamoxifen). Migration distance is expressed as the mean ± SEM of results from three independent experiments (*P < 0.05). **D,** Representative images of leading edges in a time dependent manner in moving TTFs from LH2$^{F/F}$ CAG-Cre with/without 5 μM tamoxifen. Yellow arrowheads indicate filopodia. (For interpretation of the references to colour in this figure legend, the reader is referred to the Web version of this article.)

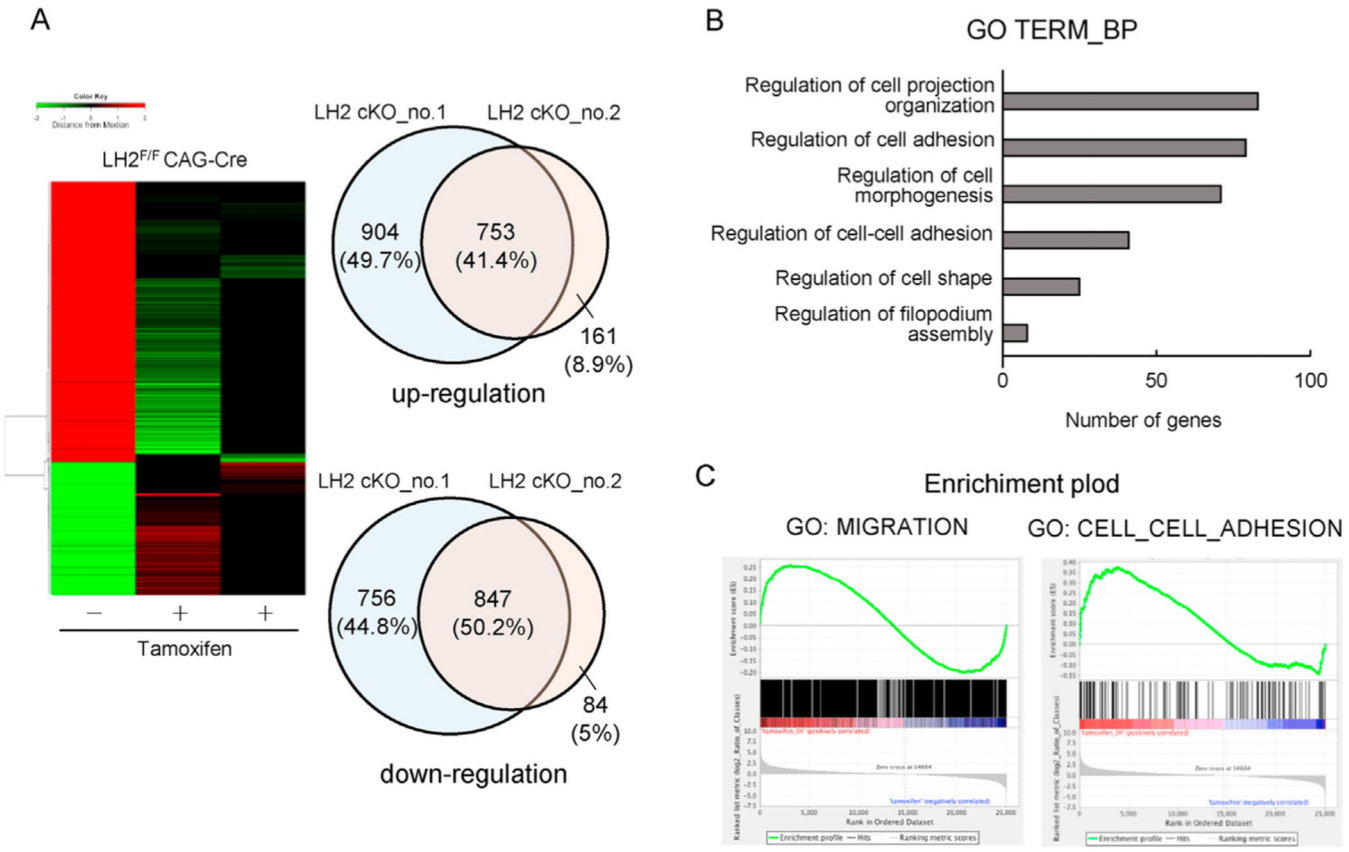

Fig. 4.

Gene expression analysis of LH2 cKO TTFs. **A,** Heat map showing results for unsupervised hierarchical clustering of selected differentially expressed genes. Venn diagrams show the percentages of differentially-expressed genes and comparison of differentially expressed genes in LH2 cKO TTFs in culture medium with tamoxifen (LH2 cKO_no.1) vs. LH2 cKO TTFs in culture medium without tamoxifen (LH2 cKO_no.2). **B,** GO term analysis of biological process showed that these genes are involved in migration activity ($P < 0.05$). **C,** GSEA of differentially expressed genes. Enrichment in genes associated with migration and cell-cell adhesion was observed (*$P < 0.05$ and FDR <0.25).